

Demonstration of extern3

An example of the deconvolutional treatment implemented in the preprocessor application “extern3” is demonstrated in this document.

Other files are assigned as follows.

File name	
00memo.txt	Measurement condition
00raw.csv	Raw experimental data
01dct.csv	Deconvolutionally treated data
cntmn.cfg	Configuration file for treating off-center Ni K emissions from Cu-target X-ray tube
dct.cfg	Main configuration file for extern3.py
xray.cfg	Configuration file for spectroscopic profile of source X-ray
axial.py	Python code for treatment of axial-divergence effect
cntmn.py	Python code for treatment of off-center Ni K emissions from Cu-target X-ray tube
dct_common.py	Python code for common subroutines used in other Python codes
equatorial.py	Python code for treatment of equatorial aberration
extern3.py	Main Python code
trnspr.py	Python code for treatment of sample-transparency effect
xray.py	Python code for treatment of spectroscopic profile of source X-ray

Example: Si (NIST SRM640d) / Rigaku MiniFlex 600-C (←)

Powder diffraction data of Si powder (NIST SRM640d) were collected with a powder diffractometer (Rigaku MiniFlex 600-C) with a silicon-strip X-ray detector (Rigaku D/teX Ultra-2). A shield tube (Canon Electronic Devices, A-21 Cu, normal focus) was used as the X-ray source. The scan rate of the measurement was $10^\circ \text{ min}^{-1}$. All the data were collected within 15 min. Further details about the sample preparation and measurement conditions are described in “00memo.txt” file in the “20191111-001” folder.

Overall intensity profiles of the observed data and the data treated with extern3 are shown in [Figure 1](#).

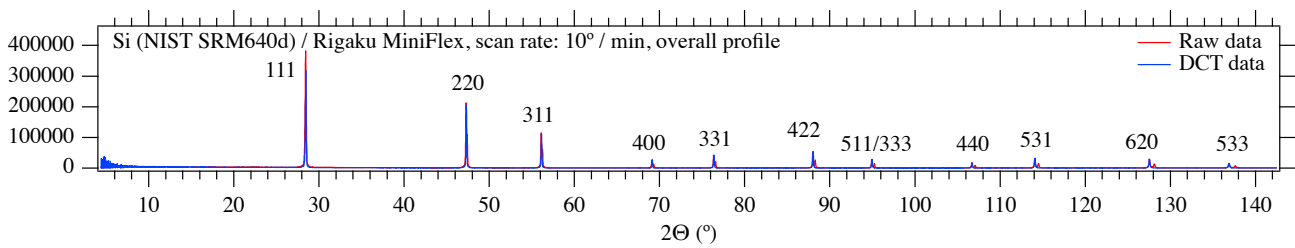


Figure 1 Overall intensity profiles of Si (NIST SRM640d) data collected with Rigaku MiniFlex 600-C, and the deconvolutionally treated (DCT) data.

The Lorentzian that corresponds to the hypothetical Cu $K\alpha_1$ peak to be convolved was set to slightly larger value (0.0003) than that used in the deconvolution process (0.000286). The values of the Lorentzian widths for deconvolution/convolution treatments are indicated in one of the configuration files “xray.cfg” for the `extern3` application. Fluctuation of the background intensity profile appears near the lower edge of the data treated with `extern3`. The Cu $K\alpha_2$ peaks, separated from Cu $K\alpha_1$ peaks at the higher diffraction angles are removed or reduced by the treatment as can be seen in [Figure 1](#).

[Figure 2](#) shows the changes of the Si 111, 422, and 533 peak profile on the deconvolutional treatment. The information values of the peak positions at 22.5°C for Cu $K\alpha_1$ X-ray, $\lambda = 1.5405929 \text{ \AA}$, listed in the NIST SRM640d certificate are indicated by arrows in each of the figures.

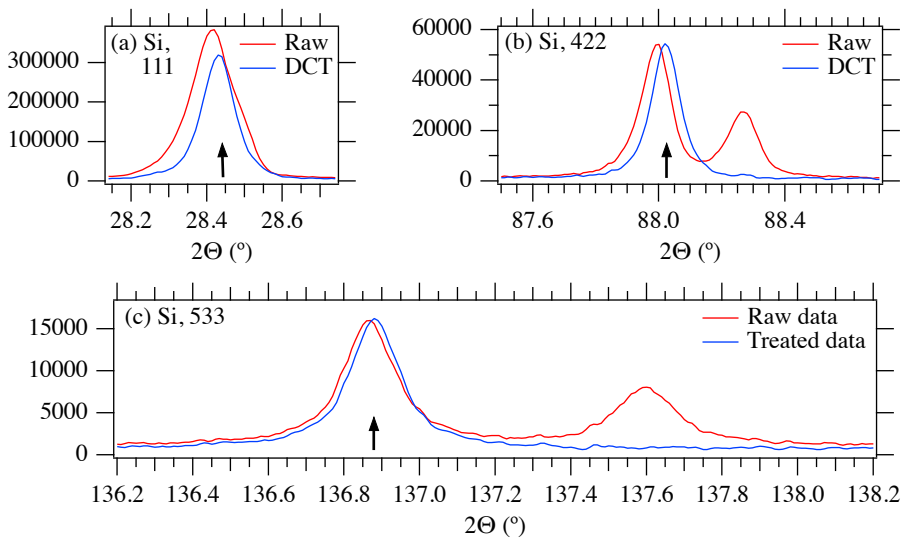


Figure 2 Si 111, 422, 533 profiles of the raw data and the deconvolutionally treated data (DCT). The information value about the diffraction angle, listed in the SRM640d certificate, is indicated by an arrow on each panel.

The peak locations of 111, 422, and 533-reflections appear to be coincided within 0.01° with the expected locations. The observed 422 peak is shifted by -0.02° from the expected location, and it is naturally assigned to the sample-transparency effect ([Figure 3.2 \(b\)](#)). The observed 533 peak profile ([Figure 3.2 \(c\)](#)) is almost symmetric, and it is naturally caused by the unusually narrow open angle (1.25°) of the Soller slits used for the measurement. The data treated by the deconvolutional method do not show significant change in the 533 peak profile.

The background profile of the data are shown in [Figure 3](#). The series of small Cu $K\beta$ peaks and step like structures caused by the Ni K -absorption edge have been removed or reduced by the deconvolutional treatment.

Misplaced Ni K emission peaks, observed for Panalytical (§1) and Philips (§2) X-ray tubes have not been found in the data collected with an X-ray tube of Canon Electronic Devices.

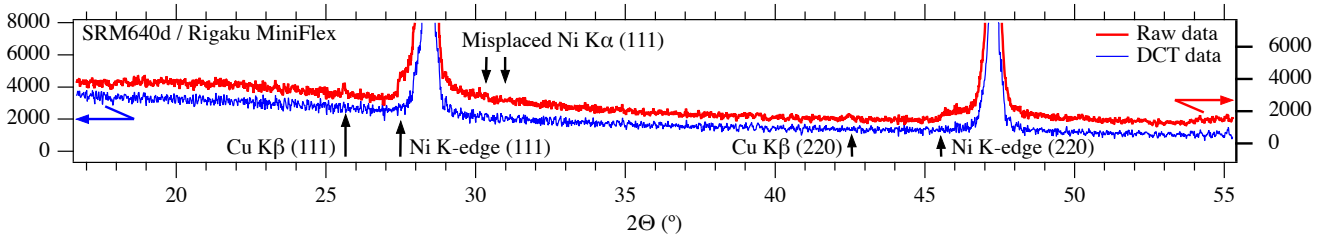


Figure 3 Background profiles of the raw data (Rigaku MiniFlex) and the deconvolutionally treated (DCT) data.

The lost intensities caused by the “spill-over” and “pass-through” effects are automatically recovered by default in the current version of `exterm3` application. The application can also offer the data of intensity correction and the first to fourth-order cumulants of the instrumental aberration functions, as optional outputs as “`cumulants_XXX.csv`” (comma separated values) file for each of the instrumental aberrations. The reported values are “ 2Θ (°), s_0 , κ_1 (°), $\kappa_2^{1/2}$ (°), $\kappa_3^{(1/3)}$ (°), $\kappa_4^{(1/4)}$ (°)”, where 2Θ (°) is the apparent diffraction angle, s_0 is the ratio of the observed intensity to the hypothetical value expected for an infinitely wide and thick specimen, and κ_k is the k -th order cumulant of each aberration function and the “reduced cumulants” for the k -th order cumulant, $\kappa_k^{(1/k)}$, (Ida *et al.*, [2018c](#)) are defined by

$$\kappa_k^{(1/k)} \equiv \text{sign}(\kappa_k) |\kappa_k|^{1/k}. \quad (3.1)$$

[Figure 4](#) shows the relative intensities affected by the “spill-over” and “pass-through” effects. It is confirmed that the Si 111 peak is not affected by the spill-over, and the intensity loss caused by the pass-through effect is less than 1% at the highest angle, while `exterm3` automatically recovers the lost intensity by default.

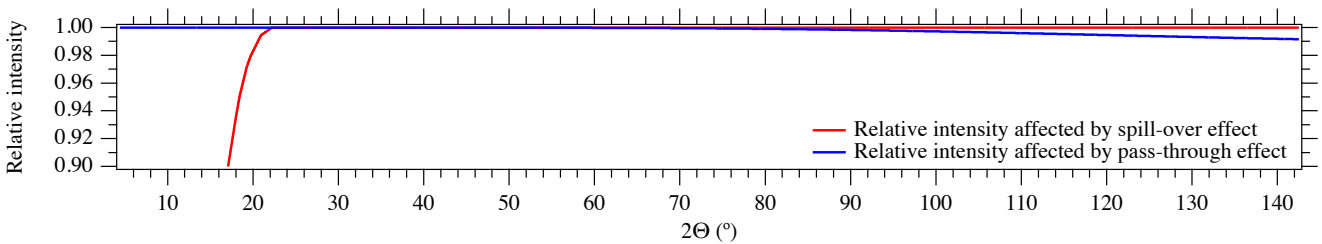


Figure 4 Relative intensities that remain from the spill-over and pass-through effects, offered as optional output from `exterm3`.

[Figure 5](#) shows the first-order cumulant κ_1 of each aberration function, which is identical to the average peak shift. The deconvolutional treatment with `exterm3` automatically corrects the average peak shift caused by those aberrations. It would not be easy to model or correct the peak shift, particularly for the component caused by the equatorial aberration about CSI-SSXD data, because the appearance of the spill-over effect is complicated for mathematical formulation, while the current

version of `exterm3` numerically evaluates the values of cumulants, based on the exact geometrical relation (Ida, 2021).

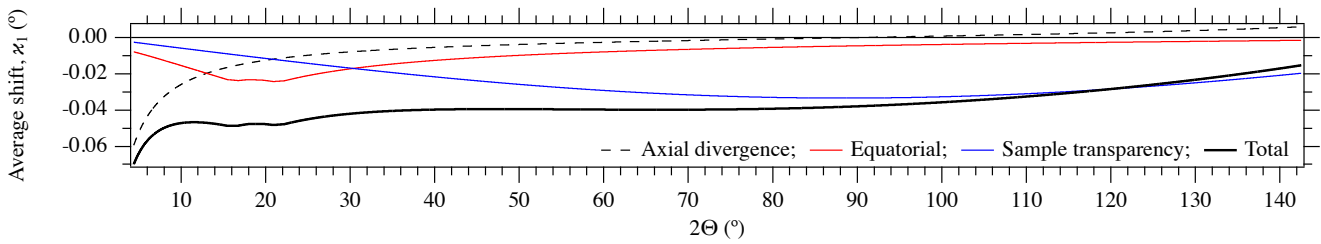


Figure 5 The first-order cumulants (average peak shift) of axial-divergence, equatorial, and sample-transparency aberrations and total peak shift.

Figure 6 shows the square root of the second-order cumulant $\kappa_2^{1/2}$ (standard deviation) of each aberration function, which can directly be related to the instrumental broadening. The deconvolutional treatment with `exterm3` do not change the values of even-order cumulants, while non-deconvolutional part of the treatment, that is, the treatment about the truncation effect of the finite thickness of the sample, may change the even-order cumulants. One should know the values of the second-order cumulants anyway, if the treated data are used for peak profile analyses. It would not be easy to model the instrumental broadening, particularly for the component caused by the equatorial aberration about CSI-SSXD data, either.

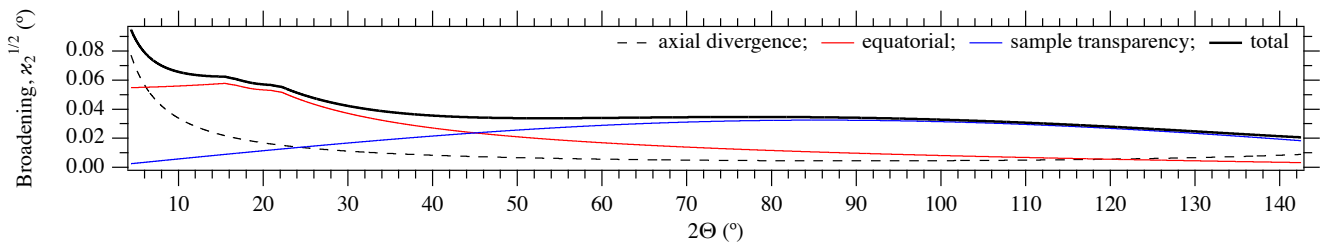


Figure 6 The square roots of the second-order cumulants (instrumental broadening) of axial-divergence, equatorial, and sample-transparency aberrations and total peak broadening.

Figure 7 shows the values of the reduced third-order cumulant $\kappa_3^{(1/3)}$ of each aberration function, which may be related to the asymmetric deformation of peak profile caused by the instrumental effect. The deconvolutional treatment with `exterm3` automatically removes the effect. It is not necessary for the users of `exterm3` to know the values of the odd-order cumulants. It would not be easy to model the asymmetric deformation of peak profile caused by the instrumental effects, particularly for the component caused by the equatorial aberration about CSI-SSXD data.

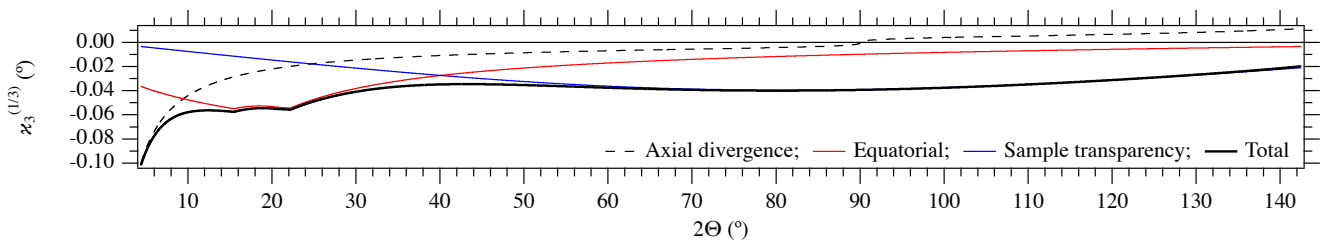


Figure 7 The reduced third-order cumulants (asymmetric profile deformation effect) of axial-divergence, equatorial, and sample-transparency aberrations and total peak broadening.

Figure 8 shows the reduced fourth-order cumulant $\kappa_4^{(1/4)}$ of each aberration function, which may be related to the sharpness of the instrumental broadening profile. The deconvolutional treatment with

term3 do not change the values of even-order cumulants, while non-deconvolutional part of the treatment, that is, the treatment about the truncation effect of the finite thickness of the sample, may change the even-order cumulants. One should know the values of the fourth-order cumulants, if the treated data are used for peak profile analyses with a model incorporating the second and fourth-order cumulants of the instrumental effect. It would not be easy to model the sharpness of the instrumental broadening profile, particularly for the component caused by the equatorial aberration about CSI-SSXD data.

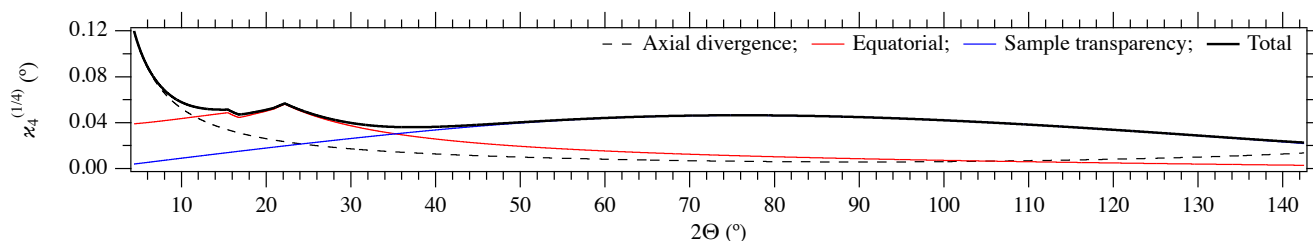


Figure 8 The reduced fourth-order cumulants (symmetric profile deformation effect) of axial-divergence, equatorial, and sample-transparency aberrations and total peak broadening.

(←)

References

- Ida, T., Ono, S., Hattan, D., Yoshida, T., Takatsu, Y. & K. Nomura. (2018a) “Deconvolution–convolution treatment on powder diffraction data collected with $\text{CuK}\alpha$ X-ray and $\text{NiK}\beta$ filter,” *Powder Diffr.* **33**, 80–87. [doi: [10.1017/S0885715618000258](https://doi.org/10.1017/S0885715618000258)]
- Ida, T., Ono, S., Hattan, D., Yoshida, T., Takatsu, Y. & K. Nomura. (2018b) “Removal of small parasite peaks in powder diffraction data by a multiple deconvolution method,” *Powder Diffr.* **33**, 108–114. [doi: [10.1017/S0885715618000337](https://doi.org/10.1017/S0885715618000337)]
- Ida, T., Ono, S., Hattan, D., Yoshida, T., Takatsu, Y. & K. Nomura. (2018c) “Improvement of deconvolution–convolution treatment of axial-divergence aberration in Bragg–Brentano geometry” *Powder Diffr.* **33**, 121–133. [doi: [10.1017/S0885715618000349](https://doi.org/10.1017/S0885715618000349)]
- Ida, T. (2020a) “Equatorial aberration of powder diffraction data collected with an Si strip X-ray detector by a continuous-scan integration method,” *J. Appl. Crystallogr.* **53**, 679–685. [doi: [10.1107/S1600576720005130](https://doi.org/10.1107/S1600576720005130)]
- Ida, T. (2020b) “Application of deconvolutional treatment to powder diffraction data collected with a Bragg-Brentano diffractometer with a contaminated Cu target and a Ni filter,” *Powder Diffr.* **35**, 166–177. [doi: [10.1017/S0885715620000445](https://doi.org/10.1017/S0885715620000445)]
- Ida, T. (2021) “Equatorial aberration for powder diffraction data collected by continuous-scan integration of a silicon strip X-ray detector,” *Powder Diffr.* **36**, 169–175. [doi: [10.1017/S0885715621000403](https://doi.org/10.1017/S0885715621000403)]
- Freiman, S. W. & Trahey, N. M. (2000) “Certificate, Standard Reference Material 640c, Silicon Powder, Line Position and Line Shape Standard for Powder Diffraction,” NIST (Gaithersburg). [url: <https://www-s.nist.gov/srmors/certificates/archive/640c.pdf>]

Keiser, D. L. & Watters, Jr., R. L. (2010) “*Certificate, Standard Reference Material 640d, Silicon Powder, Line Position and Line Shape Standard for Powder Diffraction,*” NIST (Gaithersburg).
[url: <https://www-s.nist.gov/srmors/certificates/archives/640d.pdf>]